Medicated Janus fibers fabricated using a Teflon-coated side-by-side spinneret

Deng-Guang Yu [a,*], Ying Xu [a], Miao Jin [b], Gareth R. Williams [b], Hua Zou [a],
Xia Wang [a,*], S.W. Annie Bligh [c,*]

[a] School of Materials Science & Engineering, University of Shanghai for Science and
Technology, Shanghai 200093, China.
[b] UCL School of Pharmacy, University College London, London WC1N 1AX, UK.
[c] Faculty of Science and Technology, University of Westminster, 115 New Cavendish
Street, London W1W 6UW, UK.

* Corresponding authors:
Prof. Deng-Guang, Prof. SW Annie Bligh and Prof. Xia Wang

Address:
School of Materials Science & Engineering,
University of Shanghai for Science and Technology,
516 Jungong Road, Yangpu District,
Shanghai 200093, P.R. China
Tel: +86-21-55270632
Fax: +86-21-55270632
Email: ydg017@usst.edu.cn; a.bligh@westminster.ac.uk; wangxia@usst.edu.cn

ABSTRACT:

A ~~few~~ family of medicated Janus fibers that provides ~~a~~ highly tunable biphasic drug release ~~were~~ was fabricated using a side-by-side electrospinning process employing a Teflon-coated parallel spinneret. The coated spinneret facilitated the formation of a Janus Taylor cone and in turn high quality integrated Janus structures, which could not be reliably obtained without the Teflon coating. The fibers prepared had one side consisting of polyvinylpyrrolidone (PVP) K60 and ketoprofen, and the other of ethyl cellulose (EC) and ketoprofen. To modulate and tune drug release, PVP K10 was doped into the EC side in some cases. The fibers were linear and had flat morphologies with an indent in the center. They provide biphasic drug release, with the PVP K60 side dissolving very rapidly to deliver a loading dose of the active ingredient, and the EC side resulting in sustained release of the remaining ketoprofen. The addition of PVP K10 to the EC side was able to accelerate the second stage of release; variation in the dopant amount permitted the release rate and extent ~~in the second, sustained, phase~~ this phase to be precisely tuned. These results offer the potential to rationally design systems with highly controllable drug release profiles, which can complement natural biological rhythms and deliver maximum therapeutic effects.

65

1. Introduction

A range of "top-down" nanofabrication techniques exists, but of these electrohydrodynamic atomization (EHDA, including electrospinning, electrospraying and e-jet printing) is particularly attractive because of its simplicity and capability to propagate the structure of a macroscale template into a nanostructure [1,2]. An EHDA process typically involves preparing a solution of a polymer (possibly also with a functional component) in a volatile solvent. This solution is then ejected at a precisely controlled rate from a syringe fitted with a metal needle (spinneret) towards a grounded collector plate [3-7]. A large potential difference is applied between the spinneret and collector plate. This electrical energy causes very rapid evaporation of the solvent, leading to a solid product. The spatial distribution of components in the latter mirrors that in the spinneret.

Considering a two-compartment system, the simplest structures are i) core-shell (with different interior and exterior) and ii) an asymmetric Janus structure, where the sides of the structure are different. Both can be used to develop materials with tunable or multifunctional properties. Core-shell structures, including fibers and particles, generated by EHDA have been widely explored [8,9]. These are most commonly fabricated from a concentric spinneret [10,11], although they can also be prepared using a single fluid process [12,13]. More complex structures such as three-layer nanofibers and microparticles (from tri-axial EHDA processes) and multi-compartmental structures from multiple fluid spinnerets have also been reported

87 [14,15]. However, there are very few publications reporting electrospun Janus fibers,

88 although there are hundreds on electrospun core-shell nanofibers.

89 Unlike core/shell architectures the Janus structure permits direct contact of both

90 compartments with their environment, which can be very useful in the creation of

91 multi-functional nanoscale products [16]. Such structure types are also commonly

92 found in nature [17], and Janus nanoparticles *are currently one of the one of the most*

93 *high profile topics in the nano field* [18,19~~]. In sharp contrast, very little attention has~~

94 ~~been paid to Janus fibers.~~ Since Gupta and Wilkes first reported the fabrication of

95 ~~such~~ Janus   fibers   using   side-by-side   electrospinning   with   polyvinyl

96 chloride/polyurethane and polyvinyl chloride)/polyvinylidiene fluoride [20], only a

97 very limited number of additional studies have followed their initial work [21-23].

98 This can be attributed to the difficulty of creating integrated Janus nanostructures

99 when   parallel   metal   capillaries   are   used   as   a   spinneret   for   side-by-side

100 electrospinning.

101 Biphasic controlled release of an active ingredient is much sought after in

102 pharmaceutics, particularly with an initial rapid release stage followed by sustained

103 release. Drug delivery systems (DDS) providing such release profiles can deliver an

104 effective "loading dose", producing a rapid rise in the plasma concentration of drug

105 and rapidly relieving a patient's symptoms. Subsequently, a prolonged-release phase

106 maintains an effective therapeutic concentration, avoiding repeated administrations

107 [24].

108 Different types of biphasic release DDS for potential oral administration have

109   been reported, fabricated using a wide variety of technologies [25]. Biphasic release

110   fibers from single fluid electrospinning have been generated through the encapsulation

111   of nanoparticles in the fibers [26] or the collection of different types of fibers in a

112   layer-by-layer manner [27]. However, the former method involved a complex

113   multiple-step preparation process, and the layer-by-layer collection of different fibers

114   often resulted in non-homogeneous products. Coaxial electrospinning can yield

115   biphasic release DDSs in a single step, as a result of its ability to produce materials

116   where the composition of the core and shell are different [24,25]. By changing the

117   shell-to-core fluid flow rate ratio [24] or the concentration of drug in the working fluids

118   [28], a tunable biphasic release profile with accurate control of the amount of drug

119   released in the different phases can be realized.

120   However, to date there are no reports describing the tuning of the release rate in

121   the sustained phase of release in an electrospun biphasic DDS. Being able to precisely

122   control the rate of sustained release is important to ensure the most effective and safe

123   pharmacokinetic profile for a particular disease, and to facilitate maximum absorbance

124   of the drug after oral administration. For many drugs, absorption is moderately slow in

125   the stomach, rapid in the proximal intestine, and declines sharply in the distal segment

126   of the intestine [29].

127   In this work, we aimed to develop a new side-by-side electrospinning process for

128   creating integrated Janus fibers. A new Teflon-coated spinneret was exploited to ensure

129   the two working fluids converge before they were ejected from the spinneret. A series

130   of ketoprofen-loaded Janus fibers has been prepared using poly(vinylpyrrolidone)

(PVP) K60 and ethyl cellulose (EC). The fibers exhibit biphasic drug release, with an initial burst release followed by sustained freeing of drug into solution. The release rate and extent in the second phase can be tuned by doping small amounts of PVP K10 into the EC side of the fiber systems. As a result, nanoscale drug delivery systems with highly tunable release profiles have been produced; these cannot easily be achieved using traditional pharmaceutical technologies, and thus this work offers the potential to lead to a range of new medicines and concomitant patient benefit.

2. Experimental

2.1. Materials

Polyvinylpyrrolidone K60 (PVP K60, M_w=360,000) and PVP K10 (M_w=10,000) were purchased from Sigma-Aldrich Ltd. (Shanghai, China). Ethyl cellulose (EC, 6mPa·s to 9 mPa·s) was obtained from the Aladdin Chemistry Co. Ltd. (Shanghai, China). Keteprofen (KET) was purchased from the Wuhan Fortuna Chemical Co. Ltd. (Hubei, China). Methylene blue and anhydrous ethanol were obtained from the Sinopharm Chemical Reagent Co. Ltd. (Shanghai, China). All other chemicals used were analytical grade. Water was doubly distilled immediately prior to use.

2.2. Side-by-side electrospinning

After initial optimization experiments, the solutions used for electrospinning consisted of (1) 8% (w/v) PVP K60 and 2% (w/v) KET in ethanol, and (2) 24% (w/v) EC, 2% (w/v) KET and a varied content of PVP K10 (0, 1, 2, and 5% (w/v)) in ethanol.

Two homemade side-by-side spinnerets were used for electrospinning. A flat piece of cardboard covered with aluminum foil was earthed and used as the collector

153 plate. Two syringe pumps (KDS100 and KDS200, Cole-Parmer®, Vernon Hills, IL,

154 USA) were used to drive the working fluids. A ZGF 60kV/2mA power supply

155 (Shanghai Sute Corp., Shanghai, China) was employed to provide a potential

156 difference between the spinneret and collector.

157 Electrospinning was conducted under ambient conditions (24 ± 2 °C with a

158 relative humidity of 51 ± 7 %). After optimization, the applied voltage was fixed at 12

159 kV, the fiber to collector distance at 20 cm and the flow rates of both the PVP K60 and

160 EC solutions set to 1.0 mL/h. The electrospinning processes were recorded using a

161 digital video recorder (PowerShot A490, Canon, Tokyo, Japan).

162 **2.3. Characterization**

163 *2.3.1. Morphology and structure*

164 The morphologies of the fiber products were investigated using a Quanta FEG450

165 field-emission scanning electron microscope (FESEM, FEI Corporation, Hillsboro,

166 USA). The samples were subjected to gold sputter-coating in a nitrogen atmosphere

167 prior to imaging. Average sizes (diameters for monolithic nanofibers and widths for

168 Janus fibers) were determined by measuring the fibers at more than 100 different

169 places in FESEM images, using the Image J software (National Institutes of Health,

170 Bethesda, USA).

171 The fiber structures were also studied on a JEM 2100F field-emission

172 transmission electron microscope (TEM, JEOL, Tokyo, Japan). TEM samples were

173 prepared by placing a lacey carbon-coated copper grid on the fiber collector and

174 electrospinning onto it for several minutes.

175 *2.3.2. Functional performance*

176   *In vitro* dissolution tests were conducted according to the Chinese Pharmacopoeia

177 (2010 ed.) Method II, a paddle method. Experiments were undertaken using a RCZ-8A

178 dissolution apparatus (Tianjin University Radio Factory, Tianjin, China).

179   A mass of fibers containing 40 mg KET (200, 519, 360, 370, 381 and 408 mg for

180 fibers F1, F2, F3, F4, F5 and F6, respectively) was placed in 800 mL physiological

181 saline (PS, 0.9% wt) at $37 \pm 1\,°C$, providing sink conditions with $C < 0.2C_s$. The

182 dissolution vessels were stirred at 50 rpm. At predetermined time points, 5.0 mL

183 aliquots were withdrawn from the dissolution medium and replaced with fresh PS to

184 maintain a constant volume. After filtration through a 0.22 µm membrane (Millipore,

185 Billerica, USA) and appreciate dilution with PS, the samples were analyzed at $\lambda_{max} =$

186 260 nm using a UV-vis spectrophotometer (UV-2102PC, Unico Instrument Co. Ltd.,

187 Shanghai, China). The accumulative KET released was back-calculated from the data

188 obtained against a predetermined calibration curve. All experiments were repeated six

189 times, and results given as mean $\pm$ S.D.

190 **3. Results and discussion**

191 **3.1. Implementation of the side-by-side electrospionning**

192   Traditionally, a side-by-side spinneret comprises two parallel metal capillaries.

193 Here, we used a section of Teflon tube to coat the parallel metal capillaries on their

194 outlets and project slightly over their nozzles (see the Supplementary Information, Fig.

195 S1). The Teflon coating has several advantages: 1) it can effectively prevent the

196 separation of the two working fluids, which occurs when a traditional parallel

197   spinneret is used; 2) an even distribution of charge around the spinneret is expected to

198   be achieved; 3) because Teflon is non-conductive, all the charge from the power

199   supply can be directed effectively to the working fluids [25]; 4) the non-stick nature of

200   Teflon will mean that fibers should not stick to the spinneret, and thus clogging can be

201   avoided. These factors should all facilitate the formation of a Janus Taylor cone [30].

202   **Table 1.** Details of the electrospinning processes and ~~the~~ resultant products.

No.	Process	PVP K60 side [a] Flow rate (mL/h)	EC side Flow rate (mL/h)	Composition (% w/v) EC	KET	PVP K10	Size [b] (μm)	P [c] (%)
F1	Single	1.0	--		--		0.57±0.09	20
F2	Single	--	1.0	24	2	0	0.68±0.13	7.7
F3	Side-by-side	1.0	1.0	24	2	0	0.92±0.10	11.1
F4	Side-by-side	1.0	1.0	24	2	1	1.02±0.17	10.8
F5	Side-by-side	1.0	1.0	24	2	2	0.98±0.13	10.5
F6	Side-by-side	1.0	1.0	24	2	5	1.06±0.12	9.8

203

204   [a] This fluid consisted of PVP K60 (8% w/v) and KET (2% w/v)

205   [b] Values are shown as mean ± S.D. For F1 and F2, ''size'' refers the fiber diameter, and for F3 to F6 to the full

206   width of the combined Janus fibers.

207   [c] P is the total drug content in the solid fibers calculated according to the flow rate and drug content in the fluids: P

208    $= [(F_p \times C_{pd}) + (F_e \times C_{ed})]/[(F_p \times C_{pa}) + (F_e \times C_{ea})] \times 100\%$. F_p and F_e are the flow rates of the PVP side and EC side,

209   respectively; C_{pd} and C_{ed} the drug contents in PVP and EC sides; and C_{pa} and C_{ea} the total solute content in the PVP

210   and EC solutions.

211

212   In this study six different fibers, two monolithic and four Janus, were prepared.

213   Details of the electrospinning processes are given in Table 1. The apparatus deployed

214   for side-by-side electrospinning is shown in Fig. 1a. The Teflon-coated spinneret was

215   mounted on a polypropylene syringe containing a PVP K60 solution. The syringe was

216   then placed vertically above the collector. A second syringe containing an EC solution

217   was connected to the second capillary of the spinneret *via* a flexible silicone tube. For

218   easy observation of the electrospinning processes, 0.001% (w/v) of methylene blue
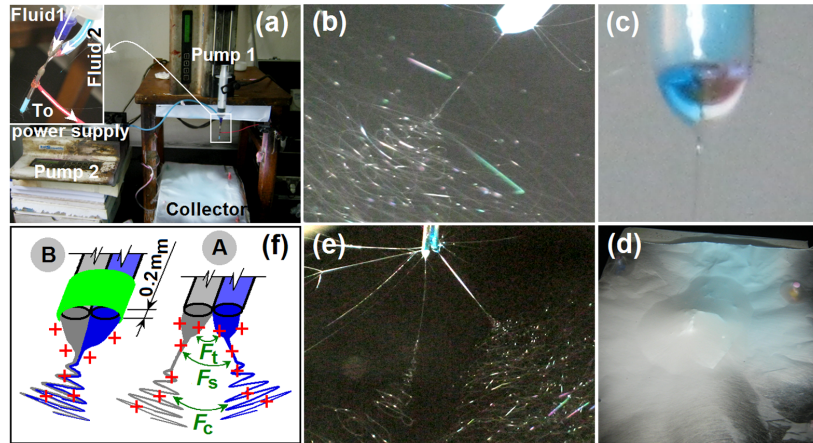
219 was added to the EC solution.

220   After a series of optimization experiments, a stable electrospinning process was

221 achieved, as depicted in Fig. 1b. A straight fluid jet was emitted from a Janus Taylor

222 cone (Fig. 1c), followed by an unstable region of bending and whipping with coils of

223 increasing size. The resultant fiber mat was light blue, with an even blue hue across

224 the product. This was attributed to the presence of methylene blue; the homogeneous

225 color distribution is indicative of an integrated Janus structure.

226   In contrast, when the process was performed without the Teflon coating the fiber

227 mat had an uneven blue color (Fig. 1d), demonstrating a failure to generate integrated

228 and homogeneous structures. The two fluids used for electrospinning were observed

229 to separate from one other immediately upon exiting the spinneret (Fig. 1e). When

230 two fluids are ejected from the nozzles of a side-by-side spinneret, there is only a very

231 small contact area between them. Since they originate in different capillaries, both

232 fluids will be charged prior to coming into contact and thus it is inevitable that they

233 will repel one another, preventing them from converging to form a Janus Taylor cone;

234 this is illustrated in Fig. 1f(A). This initial repulsive force, F_t, leads to two Taylor

235 cones; it is then followed by further repulsion between the two straight fluid jets (F_s)

236 and the two bending and whipping coils (F_c). These factors result in the failure to

237 form integrated Janus structures. When the spinneret was coated with Teflon (Fig.

238 1f(B)), the two fluids are found to first converge, before forming a compound Taylor

239 cone and ultimately resulting in integrated Janus structures.

240

241

Fig. 1. The side-by-side electrospinning process: (a) The experimental apparatus (inset: the connection of the side-by-side spinneret with the working fluids and power supply); (b) a photograph of a typical side-by-side electrospinning process with the Teflon-coated spinneret; (c) a Janus Taylor cone formed with the Teflon-coated spinneret; (d) the fiber mat from side-by-side electrospinning with the uncoated side-by-side spinneret; (e) the separation of fluids when using the uncoated spinneret; (f) an illustration of the role played by the Teflon coating: A - the separation of fluids arising from repulsive forces F_t (between the two Taylor cones), F_s (between the two straight fluid jets) and F_c (between the two coils); and B - the formation of an integrated Janus Taylor cone with the Teflon coating.

3.2. Morphologies and structures of the fabricated Janus nanofibers

First, the monolithic fibers F1 and F2 were prepared by single fluid

electrospinning using the traditional side-by-side spinneret with one fluid turned off.

Both fluids individually were found to have good electrospinnability. FESEM images

of F1 (PVP K60 and KET) are shown in Fig. 2a. The fibers have a linear morphology

and smooth surfaces, and an average diameter of 0.57 ± 0.09 µm. The FESEM images

of F2 (EC and KET) are depicted in Fig. 2b; again the fibers are smooth and linear,

possessing an average diameter of 0.68 ± 0.13 µm.

The FESEM images of the Janus fibers F3, F4, F5 and F6 are exhibited in Fig. 2c

to Fig 2f. All have linear morphologies and smooth surfaces. While the monolithic

fibers are cylindrical in shape, these fibers have a flat concave topography but are still

linear and smooth. The two sides of the fibers can clearly be resolved. The fiber

diameters can be found in Table 1. F4 to F6 contain small amounts of PVP K10 doped

into the EC side of the fibers, but this is found to have no significant influence on

their size or morphology.
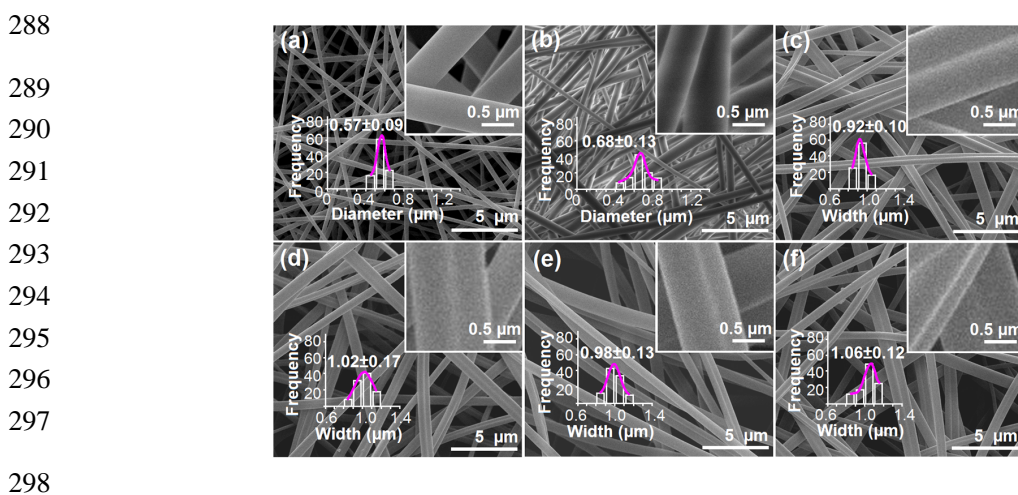
Fig. 2. FESEM images of the fibers, together with their size distributions: (a) F1

(drug-loaded PVP fibers); (b) F2 (drug-loaded EC fibers); and the Janus PVP/EC/KET

fibers (c) F3; (d) F4; (e) F5; (f) F6.

302　　　　TEM images of F3, F4, F5 and F6 are displayed in Fig. 3a to Fig. 3d. Two

303　different sides to the fibers can again be discerned, with the larger and slightly darker

304　side being the EC compartment. In the TEM image of F3 (Fig. 3a), there is a central

305　region with a lower contrast level, suggesting a concave topography. F4 (Fig. 3b)

306　shows forks resulting from separation of the two sides of the fiber.
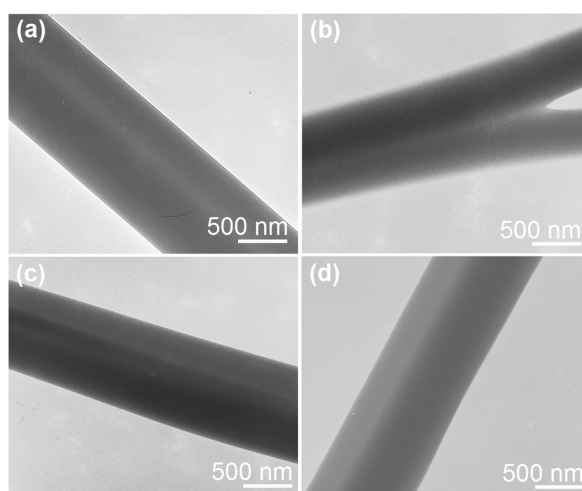
307
308
309
310
311
312
313
314
315
316
317

318
319　　　　　　　**Fig. 3.** TEM images of (a) F3; (b) F4; (c) F5; (d) F6.

320　**3.3. *In vitro* dissolution tests**

321　　　　All the ~~prepared six types of~~ fibers are polymeric composites with KET

322　present~~ing~~ in an amorphous ~~status~~ state due to the the existence of hydrogen bonding

323　and hydrophobic interactions between the drug and its carrier (see the Supplementary

324　Information, Figs. S2 to S4). In the *in vitro* dissolution tests, the monolithic PVP

325　fibers F1 provide a very fast drug release profile, freeing all the loaded drug within

326　one minute (Fig. 4a and Table 2). This can be attributed to the large surface area and

327　small diameter of the individual nanofibers, the porous 3D web structures of the fiber

328　mats, the highly hydrophilic and fast-dissolving nature of PVP, and the amorphous

329　state of KET in the fibers. In contrast, the F2 (EC) fibers give a sustained release

330   profile (Fig. 4a and Table 2), with release of 10.7% and 33.4% in the first minute and

331   first hour, respectively. After 24 h, 82.5% of the embedded KET has been released.

332   The Janus fibers F3 to F6 result in biphasic drug release profiles, with ~~part~~ a portion

333   of the embedded drug being released rapidly into the dissolution medium with the

334   dissolution of the PVP side of the fibers. Subsequently, the EC side of the fibers leads

335   to sustained release of KET (Fig. 4a and Table 2). The addition of small amounts of

336   PVP K10 to the EC side of the fibers permits the release in the second, sustained,

337   phase to be tuned. An increase in PVP K10 content causes the release rate and the

338   percentage released after 24h to increase correspondingly (Fig. 4b and Table 2). The

339   F6 fibers, with 16.1% w/w PVP K10 in the EC side, released all the incorporated drug

340   within 16 h.

341   The second phase of the *in vitro* dissolution data (up to 16 h) was analyzed using

342   the zero-order equation and Peppas equations:

343   Zero-order equation [31]: $Q_z = a + r\, t_z$

344   (where Q_z is the release percentage, t_z is the time, a is a constant and r is the release

345   rate).

346   Peppas equation: $Q_p = kt_p^{\,n}$

347   (where Q_p is the release percentage, t_p is the time, k is a constant and n is an exponent

348   that indicates the release mechanism).

349   The results of this analysis are shown in Table 2. Release from the EC side of the

350   fibers appears to follow a typical Fickian diffusion mechanism; the values of the

351   exponent n are all smaller than 0.45. The zero-order equation provides a simple way

to compare the release rate (r) from the EC side of the different Janus fibers. As the content of PVP K10 (C) in the EC side was increased from 0% to 3.7%, 7.1% and 16.1% w/w, the r values increased correspondingly from 2.16, to 2.31, 2.38 and 2.65 h^{-1}, respectively. A linear relationship can be established: $r = 2.1756+0.0297C$ (R=0.9964; Fig. 4b). This demonstrates that the drug release rate from the EC matrix can be easily manipulated through doping with hydrophilic PVP K10.
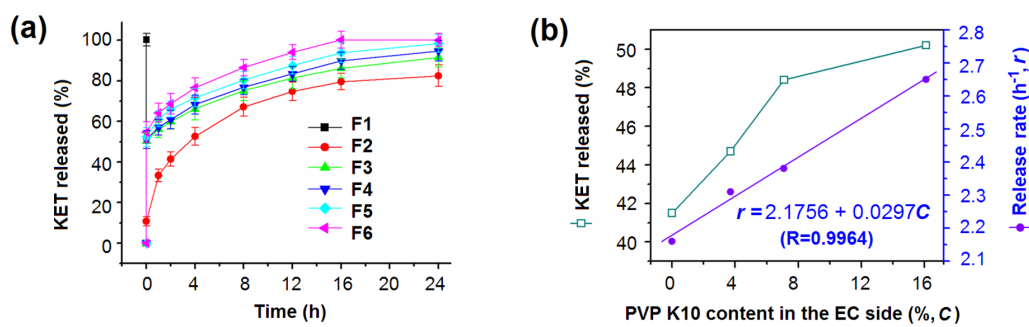
Fig. 4. The release of KET from the electrospun nanofibers: (a) the *in vitro* KET release profiles from the six fibers; **(b)** the variation of the release percentage and rate in the second phase as a function of the PVP K10 content in the EC side of the fibers.

Table 2. Data on the release of KET from the drug-loaded fibers [a,b] (n=6).

| Fiber | First phase (1 min, %) | Rel after 24 h (%) | Second phase of release | | |
| | | | Rel[c] (%) | Regressed equation (to 16h) | |
				Peppas	Zero-order
F1	100±2.8	--	--	--	--
F2	10.7±2.2	82.5±5.3	--	$Q_{p2}=33.46t_{p2}^{0.3252}$ (R$_{p2}$=0.9982)	--
F3	50.4±3.9	91.5±4.7	41.1 (41.5)	$Q_{p3}=54.61t_{p3}^{0.1576}$ (R$_{p3}$=0.9921)	$Q_{z3}=54.62+2.16t_{z3}$ (R$_{z3}$=0.9773)
F4	51.4±4.4	94.7±5.1	43.3 (44.7)	$Q_{p4}=55.54t_{p4}^{0.1621}$ (R$_{p4}$=0.9932)	$Q_{z4}=55.44+2.31t_{z4}$ (R$_{z4}$=0.9798)
F5	52.3±4.7	98.4±4.3	46.1 (48.4)	$Q_{p5}=59.78t_{p5}^{0.1525}$ (R$_{p5}$=0.9899)	$Q_{z5}=58.71+2.38t_{z5}$ (R$_{z5}$=0.9710)
F6	54.7±5.2	100.2±3.2	45.5	$Q_{p6}=62.53t_{p6}^{0.1624}$	$Q_{z6}=61.61+2.65t_{z6}$

374

375   [a] The burst release in the first minute is defined as the first phase, and the data between the first minute and 16h

376   were used to determine the drug release equations.

377   [b] Abbreviations: Q_{p2}, t_{p2}, and R$_{p2}$ refer to the release percentage, time and correlation coefficient calculated with the

378   Peppas equation for F2. Q_{z2}, t_{z2}, and R$_{z2}$ are the release percentage, time and correlation coefficient determined with

379   the zero-order equation for nanofibers F2. Quantities are defined similarly for the other fibers; the numerical

380   subscript gives the identity of the fiber sample under consideration.

381   [c] The percentage released in the second phase was calculated by subtracting the percentage of drug released in the

382   first stage from the release percentage after 24 h. The values in brackets represent the percentage of the total

383   amount of drug release which came from the EC sides (i.e. the drug content released after 24 h minus 50%, the

384   amount of drug in the PVP side of the fibres).

385   **3.4. Drug release mechanism**

386   To investigate the drug release mechanism, samples were recovered from the

387   dissolution apparatus after 24h and dried in air. The SEM results, shown in Fig. 5a to

388   5d, show the morphologies of the EC side of the fibers (the PVP side dissolves

389   completely in a few seconds). Although the overall Janus fibers did not appear to be

390   affected by the addition of PVP K10 to the EC side, the size of the fibers recovered

391   after 24h of dissolution appears to decrease with an increase of PVP K10 content, and

392   they have increasingly curved morphologies (see the Supplementary Information, Fig.

393   S5). The remnant nanofibers had rough and wrinkled surfaces, displaying holes and

394   grooves; larger PVP K10 contents appear to promote more of these features.
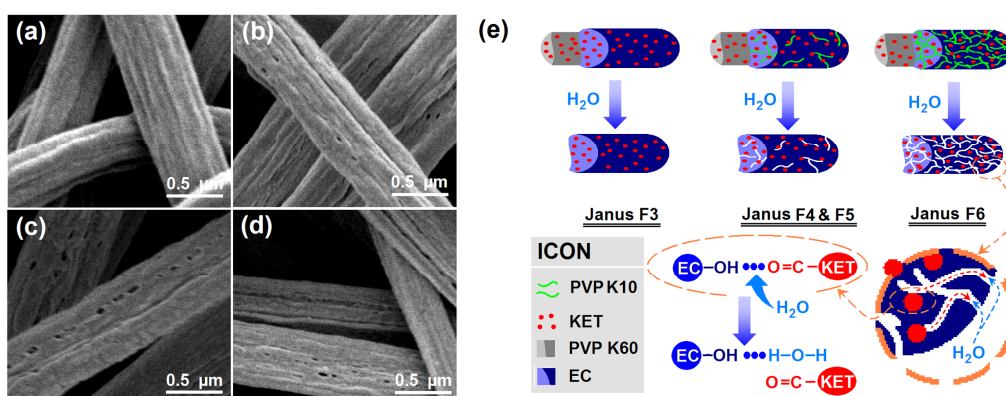
395

396

397

398

399

400

401

402

403

404

Fig. 5. FESEM images of the fibers remaining after 24h of dissolution and the proposed drug release mechanism. (a) to (d) show the remains of fibers F3 to F6 respectively; (e) is a schematic diagram explaining the mechanism of drug release from the Janus fibers.

A potential mechanism underlying the biphasic release profile is given in Fig. 5e. After encountering water, the PVP K60 side of the Janus fibers will dissolve very rapidly and immediately free all the drug it contains. The remaining EC side provides the sustained release phase. When there is no PVP K10 in the EC side, as the case of F3, water diffuses into the EC matrix very slowly. KET is a poorly water soluble drug, and thus the dissolution of KET and its diffusion from the interior of the fibers to the dissolution medium proceed very slowly. Because EC is totally insoluble in water, it is inevitable that a certain amount of KET will remain trapped in the fibers and cannot be released even after 24h.

The PVP K10 doped in the EC side of the fibers is highly soluble in water, and thus will dissolve rapidly on encountering water. As it does so, it will generate holes and pores in the EC matrix. The presence of increased amounts of PVP K10 will enhance this effect. The pores formed after dissolution of PVP K10 will facilitate the diffusion of water to the interior of the EC matrix, and of KET molecules into the dissolution media. This in turn increases the drug release rate and amount in the second phase of release. Further increases of PVP K10 content will yield interconnected pores, further aiding the movement of water into and drug out of the inside of the fibers, as is the case in for the Janus fibers F6 (Fig. 5d).

427   As a counterpart of the core-shell structure, the Janus structure can be exploited

428   to develop a wide variety of functional and multi-functional nanomaterials [32]. The

429   side-by-side electrospinning process reported here is easy to undertake, and our

430   results should expand the possibilities for exploiting electrospinning to fabricate novel

431   functional nanocomposites with Janus morphology. There are many possibilities for

432   the use of such materials in developing new biomedical materials, in addition to the

433   tunable biphasic release systems reported here. For example, the fibers could be

434   exploited to develop systems permitting the controlled release of multiple drugs for a

435   combined therapy, or for new wound dressings with one side providing adhesive and

436   anti-inflammatory functions and the other providing sustained release of the active

437   ingredients required for wound healing. By collecting Janus nanofibers in an aligned

438   [33] or layer-by-layer fashion [34] additional strategies can be conceived for

439   generating novel structures and building new structure-property-activity relationships.

440   Furthermore, coaxial electrospinning allows the field of materials which can be

441   electrospun to be broadened considerably, as often electrospinning can be achieved

442   with only one of the two working fluids being electrospinnable on its own [35].

443   Similarly, it might be possible to implement side-by-side electrospinning using one

444   spinnable and one unspinnable fluid. This possibility is being studied at present. Much

445   work has been undertaken to explore the scalability of single-fluid electrospinning

446   [36,37], with very promising results. Hence, the generation of Janus fibers on a large

447   scale should be eminently possible, and the novel nanoscale DDS which can be

448   generated using such fibers have the real possibility for clinical translation [38].

4. Conclusion

In summary, here we developed a Teflon-coated spinneret which could be used for ~~produced~~ highly effective and stable side-by-side electrospinning. The use of a Teflon coating can effectively prevent the separation of the two working fluids seen when attempting electrospinning with no coating. A series of medicated Janus fibers was successfully fabricated; these ~~comprised two~~ had two distinct sides respectively made of poly(vinylpyrrolidone) (PVP) K60 and ethyl cellulose (EC), loaded with ketoprofen (KET) as a model active ingredient. PVP K10 was added to the EC side of the fibers in some cases~~,~~ to act as a porogen. Electron microscopy ~~SEM and TEM~~ images clearly demonstrated that integrated Janus fiber structures were produced, in which the KET was found to be amorphously distributed. *In vitro* dissolution tests demonstrated that all the Janus fibers were able to provide a biphasic controlled release profile, with an initial burst followed a slower and sustained release phase. By varying the amount of PVP K10 doped in the EC side of the fibers, the release rate and total release percentage can be precisely tuned. Our results proffer a platform for designing novel drug delivery systems that can provide a tunable release profile designed to complement natural biological rhythms for maximum therapeutic effects.

References

471 [1] S. Agarwal, A. Greiner, J.H. Wendorff, Prog. Polym. Sci. 38 (2013) 963.

472 [2] P. Tonglairoum, T. Ngawhirunpat, T. Rojanarata, R. Kaomongkolgit, P.

473 Opanasopit, Colloids Surf. B 126 (2015) 18.

474 [3] W. Liu, Z. Wu, Y. Wang, Z. Tang, J. Du, L. Yuan, D. Li, H. Chen, J. Mater. Chem.

475 B 2 (2014) 4272.

476 [4] Z. Tang, D. Li, X. Liu, Z. Wu, W. Liu, J.L. Brash, H. Chen, Polym. Chem. 4

477 (2013) 1583.

478 [5] W. Yang, J. Fu, D. Wang, T. Wang, H. Wang, S. Jin, N. He, J. Biomed.

479 Nanotechnol. 6 (2010) 254.

480 [6] X. Ji, T. Wang, L. Guo, J. Xiao, Z. Li, L. Zhang, Y. Deng, N. He, J. Biomed.

481 Nanotechnol. 9 (2013) 417.

482 [7] Z. Aytac, S.Y. Dogan, T. Tekinay, T. Uyar, Colloids Surf. B 120 (2014) 125.

483 [8] Q. Shi, Q. Fan, W. Ye, J. Hou, S.C. Wong, X. Xu, J. Yin, Colloids Surf. B 125

484 (2015) 28.

485 [9] T. Wang, X. Ji, L. Jin, Z. Feng, J. Wu, J. Zheng, H. Wang, Z.W. Xu, L. Guo, N.

486 He, ACS Appl. Mater. Interfaces 5 (2013) 3757.

487 [10] X. Ji, W. Yang, T. Wang, C. Mao, L. Guo, J. Xiao, N. He, J. Biomed.

488 Nanotechnol. 9 (2013) 1672.

489 [11] W. Wang, Z. Li, T. Jiang, Z. Zhao, Y. Li, Z. Wang, C. Wang, ACS Appl. Mater.

490 Interfaces 4 (2012) 6080.

491 [12] A.V. Bazilevsky, A.L. Yarin, C.M. Megaridis, Langmuir 23 (2007) 2311.

492 [13] X. Xu, X. Zhuang, X. Chen, X. Wang, L. Yang, X. Jing, Macromol. Rapid

493   Commun. 27 (2006) 1637.

494   [14] D.G. Yu, X. Li, X. Wang, J. Yang, S.W.A. Bligh, G. Williams, ACS Appl. Mater.

495   Interfaces 7 (2015) 18891.

496   [15] Z. Ahmad, H.B. Zhang, U. Farook, M. Edirisinghe, E. Stride, P. Colombo, J. R.

497   Soc. Interfaces 5 (2008) 1255.

498   [16] W. Chen, Z. Ma, X. Pan, Z. Hu, G. Dong, S. Zhou, M. Peng, J. Qiu, J. Am.

499   Ceram. Soc. 97 (2014) 1944-1951.

500   [17] S. Jiang, S. Granick, (Ed.): Janus particle synthesis, self-assembly and

501   applications (RSC) 2012, p5-p15.

502   [18] J. Hu, S. Zhou, Y. Sun, X. Fang, L. Wu, Chem. Soc. Rev. 41 (2012) 4356.

503   [19] A. Walther, A. H. E. Müller, Chem. Rev. 113 (2013) 5194.

504   [20] P. Gupta, G. L. Wilkes, Polymer 44 (2003) 6353.

505   [21] G. Chen, Y. Xu, D.G. Yu, D.F. Zhang, N.P. Chatterton, K.N. White, Chem.

506   Commun. 51 (2015) 4623.

507   [22] J.D. Starr, J.S. Andrew, Chem. Comm. 49 (2013) 4151.

508   [23] J.D. Starr, M. A.K. Budi, J.S. Andrew, J. Am. Ceram. Soc. 98 (2015) 12.

509   [24] D.G. Yu, X. Wang, X.Y. Li, W. Chian, Y. Li, Y.Z. Liao, Acta Biomater. 9 (2013)

510   5665.

511   [25] D.G. Yu, F. Liu, L. Cui, Z.P. Liu, X. Wang, S.W.A. Bligh, RSC Adv. 3 (2013)

512   17775.

513   [26] B. Song, C. Wu, J. Chang, Acta Biomater. 8 (2012) 1901.

514   [27] L.Y. Huang, C. Branford-White, X.X. Shen, D.G. Yu, L.M. Zhu, Int. J. Pharm.

515 436 (2012) 88.

516 [28] W. Qian, D.G. Yu, Y. Li, Y.Z. Liao, X. Wang, L. Wang, Int. J. Mol. Sci. 15 (2014)

517   774.

518 [29] P.K. Gupta, J.R. Robinson, Oral Controlled-release delivery. In: A. Kydonieus,

519   (Ed.), Treatise on controlled drug delivery. Marcel Dekker, New York, 1992,

520   pp.255-313.

521 [30] C. Li, Z.H. Wang, D.G. Yu. Colloids Surf. B 114 (2014) 404.

522 [31] N.A. Peppas, Pharm Acta Hel 60 (1985)110.

523 [32] S. Venkataraman, J.L. Hedrick, Z.Y. Ong, C. Yang, P.L. Rachel Ee, P.T.

524   Hammond, Y.Y. Yang. Adv. Drug Del. Rev. 63 (2011) 1228.

525 [33] J. Xie, W. Liu, M.R. MacEwan, P.C. Bridgman, Y. Xia, ACS Nano 8 (2014)

526   1878.

527 [34] B. Zhou, Y. Li, H. Deng, Y. Hu, B. Li, Colloids Surf. B 116 (2014) 432.

528 [35] Y.H. Wu, D.G. Yu, X.Y. Li, A.H. Diao, U.E. Illangakoon, G.R. Williams, J. Mater.

529   Sci. 50 (2015) 3604.

530 [36] F. Yener, O. Jirsak, J. Nanomater. 2012 (2012) 839317.

531 [37] Z.K. Nagy, A. Balogh, B. Démuth, H. Pataki, T. Vigh, B. Szabó, K. Molnár, B.T.

532   Schmidt, P. Horák, G. Marosi, G. Verreck, I. Van Assche, M.E. Brewster, Int. J.

533   Pharm. 480 (2015) 137.

534 [38] B. Démuth, Z.K. Nagy, A. Balogh, T. Vigh, G. Marosi, G. Verreck, I. Van Assche,

535   M.E. Brewster, Inter. J. Pharm. 486 (2015) 268.

536

537

538

539

540

541

542

543

Captions of Tables and Figures

Table 1. Details of the electrospinning processes and ~~the~~ resultant products.

Table 2. Data on the release of KET from the drug-loaded fibers [a,b] (n=6).

Fig. 1. The side-by-side electrospinning process: (a) the experimental apparatus (inset: the connection of the side-by-side spinneret with the working fluids and power supply); (b) a photograph of a typical side-by-side electrospinning process with the Teflon-coated spinneret; (c) a Janus Taylor cone formed with the Teflon-coated spinneret; (d) the fiber mat from side-by-side electrospinning with the uncoated side-by-side spinneret; (e) the separation of fluids when using the uncoated spinneret; (f) an illustration of the role played by the Teflon coating: A - the separation of fluids arising from repulsive forces F_t (between the two Taylor cones), F_s (between the two straight fluid jets) and F_c (between the two coils); and B - the formation of an integrated Janus Taylor cone with the Teflon coating.

Fig. 2. FESEM images of the fibers, together with their size distributions: (a) F1 (drug-loaded PVP fibers); (b) F2 (drug-loaded EC fibers); and the Janus PVP/EC/KET fibers (c) F3; (d) F4; (e) F5; (f) F6.

Fig. 3. TEM images of (a) F3; (b) F4; (c) F5; (d) F6.

560   **Fig. 4.** The release of KET from the electrospun nanofibers: (a) the *in vitro* KET release

561   profiles from the six fibers; (b) the variation of the release percentage and rate in the second

562   phase as a function of the PVP K10 content in the EC side of the fibers.

563   **Fig. 5.** FESEM images of the fibers remaining after 24h of dissolution and the proposed drug

564   release mechanism. (a) to (d) show the remains of fibers F3 to F6 respectively; (e) is a

565   schematic diagram explaining the mechanism of drug release from the Janus fibers.

566